CHEMISTRY
A EUROPEAN JOURNAL

ChemPubSoc Europe

DOI: 10.1002/chem.201302028

Formation and Geometrical Control of Polygon-Like Metal-Coordination Assemblies

Hiromitsu Maeda,*[a] Ryo Akuta,[a] Yuya Bando,[a] Kazuto Takaishi,[b, c] Masanobu Uchiyama,[b, d] Atsuya Muranaka,[b, e] Norimitsu Tohnai,[e, f] and Shu Seki*[g]

Abstract: Polygon-like [2+2]- and [3+3]-type metal complexes were prepared from dipyrrin dimers connected by acute-angled spacers. The electrical conduction depends strongly on the packing alignment of the compounds, revealing the presence of effective hopping pathways for holes with relatively high mobility up to 0.11 $cm^2V^{-1}s^{-1}$ along the aligned axis of [3+3]-type metal-bridged assemblies. These observations correlated with the geometrical control of the π-conjugated metal complexes in the cyclic structures, which enables their ordered arrangement in the assemblies.

Keywords: cyclic compounds · electrical conduction · N ligands · pyrrole derivatives · supramolecular chemistry · X-ray diffraction

Introduction

The formation of polygon-like metal-coordination assemblies of π-conjugated molecules is significant for fabricating highly ordered structures that serve as electronic and optoelectronic materials, such as 1D stacking columns in soft materials, 2D patterns on substrates, and 3D organized structures in crystals.[1,2] In contrast to polyhedral metal complexes, disk-like polygons seem to be suitable as structural subunits for the construction of target dimension-controlled structures. It is evident that geometrical control of the metal-assisted polygons tunes the organized structures and properties of the metal-organic materials. Furthermore, the control of the number and shape of constituting of metal-coordination polygons can be achieved by the design and synthesis of π-conjugated molecules consisting of multiple ligand moieties and spacer units. A candidate ligand component is dipyrrin (dipyrromethene), which acts as a monoanionic bidentate ligand and, as a result, balances the positive charges of metal cations to afford electronically neutral metal complexes.[3] Dipyrrin is a π-conjugated ligand molecule that exhibits photo-absorption in the visible region. Thus far, dimeric dipyrrins connected by phenylethynyl spacers of rod-like and obtuse-angled shapes were found to form dispersed coordination polymers along with discrete macrocycles by complexation with metal cations such as Zn^{II} and Ni^{II}.[4] Based on the previous studies, appropriately designed acute-angled spacers would give cyclic metal-coordination assemblies because of the preorganized orientations of coordination sites with a corresponding negligibly small entropy loss. In this paper, we report the formation of dipyrrin-based polygon-like metal-coordination assemblies, which showed electrical conductive properties in the crystal state, wherein the polygons are located in ordered arrangements.

Results and Discussion

Metal-bridged dipyrrin-based polygon-like structures were constructed by using various combinations of ligand molecules and metal ions. Initially, acute-angled dipyrrin dimer **1a** and α-methyl-substituted **1b** (Figure 1, top) were synthesized by the ordinary procedures described in the literatur-

[a] Prof. Dr. H. Maeda, R. Akuta, Dr. Y. Bando
College of Pharmaceutical Sciences
Ritsumeikan University, Kusatsu 525-8577 (Japan)
Fax: (+81) 77-561-2659
E-mail: maedahir@ph.ritsumei.ac.jp

[b] Dr. K. Takaishi, Prof. Dr. M. Uchiyama, Dr. A. Muranaka
Advanced Elements Chemistry Research Team
RIKEN-ASI, Wako 351-0198 (Japan)

[c] Dr. K. Takaishi
Faculty of Science and Technology
Seikei University, Musashino 180-8633 (Japan)

[d] Prof. Dr. M. Uchiyama
Graduate School of Pharmaceutical Sciences
The University of Tokyo, Tokyo 113-0033 (Japan)

[e] Dr. A. Muranaka, Prof. Dr. N. Tohnai
PRESTO (Japan) Science and Technology Agency (JST)
Kawaguchi 332-0012 (Japan)

[f] Prof. Dr. N. Tohnai
Department of Material and Life Science
Graduate School of Engineering, Osaka University
Suita 565-0871 (Japan)

[g] Prof. Dr. S. Seki
Department of Applied Chemistry
Graduate School of Engineering, Osaka University
Suita 565-0871 (Japan)
Fax: (+81) 6-6879-4586
E-mail: seki@chem.eng.osaka-u.ac.jp

Supporting information for this article is available on the WWW under http://dx.doi.org/10.1002/chem.201302028.

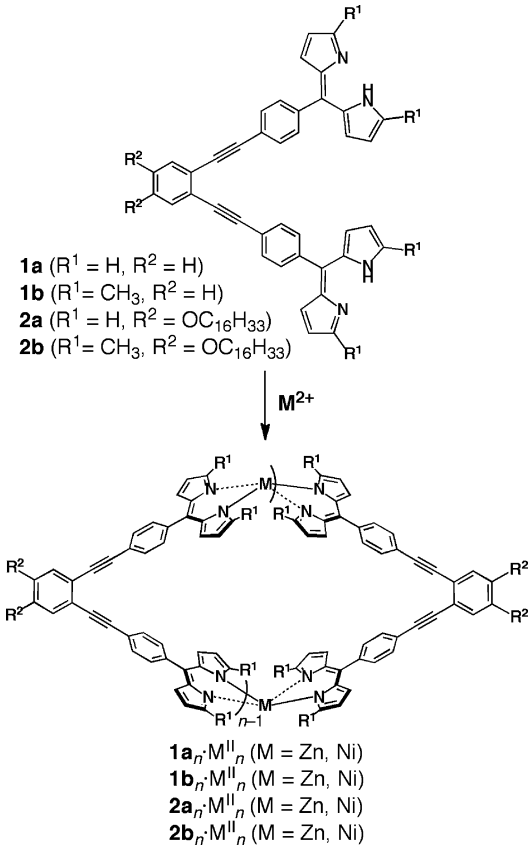

Figure 1. Formation of cyclic metal complexes from acute-angled dipyrrin dimers **1a**,**b** and **2a**,**b**.

e.[4a] Treatment of **1a** with $Zn(OAc)_2{\cdot}2H_2O$ afforded Zn^{II} complexes as orange precipitates from various solvents, such as $CHCl_3$, THF, and CH_3CN. ESI-TOF-MS of the Zn^{II} complex at $m/z = 1359.16$ indicated the formation of [2+2]-type complex $\mathbf{1a}_2{\cdot}Zn^{II}_2$ (Figure 1, bottom) and not the [3+3]-type complex $\mathbf{1a}_3{\cdot}Zn^{II}_3$ (Table 1), which was expected from the geometry of the spacer unit. The ^{1}H NMR spectrum of $\mathbf{1a}_2{\cdot}Zn^{II}_2$ in $CDCl_3$ (Figure 2a) exhibited signals at $\delta = 7.41$ and 6.61/6.11 ppm for pyrrole α- and β-positions, respectively. Such symmetrical patterns suggested that the conformational change at the orthogonally arranged dipyrrin moieties around Zn^{II} was fast at the NMR timescale. Under dilute complexation conditions, a mixture of $\mathbf{1a}_2{\cdot}Zn^{II}_2$ and a higher oligomer $\mathbf{1a}_3{\cdot}Zn^{II}_3$ were formed. Interestingly, the higher oligomers were gradually transformed into $\mathbf{1a}_2{\cdot}Zn^{II}_2$, which was confirmed by ^{1}H NMR spectral changes, wherein the integral $\mathbf{1a}_2{\cdot}Zn^{II}_2/\mathbf{1a}_3{\cdot}Zn^{II}_3$ ratio of 2:3 that was found immediately after dissolving in $CDCl_3$ was changed to 5:1 after 5 h. In this system, only $\mathbf{1a}_2{\cdot}Zn^{II}_2$ can be isolated and purified, even though $\mathbf{1a}_2{\cdot}Zn^{II}_2$ is less stable than $\mathbf{1a}_3{\cdot}Zn^{II}_3$ as suggested by theoretical analysis.[5] The relative stability per $\mathbf{1a}{\cdot}Zn^{II}$ moiety in $\mathbf{1a}_3{\cdot}Zn^{II}_3$ compared with $\mathbf{1a}_2{\cdot}Zn^{II}_2$, estimated by DFT calculation at the B3LYP/6–31G(d,p) level, is 2.63 kcal mol^{-1}, suggesting that an entropic factor may be contributing to the predominant formation of $\mathbf{1a}_2{\cdot}Zn^{II}_2$.

Table 1. Isolated yields (%) of metal complexation by dipyrrin dimers.

Ligands	Zn^{II} complexes		Ni^{II} complexes	
	[2+2]	[3+3]	[2+2]	[3+3]
1a	60	–[a]	72	–[a]
1b	13	24	9	32
2a	–[b]	–[b]	–[b]	–[b]
2b	36	27	15	24

[a] Not isolated. [b] Not isolated due to the formation of complicated mixtures.

On the other hand, as summarized in Table 1, compound **1b** afforded a [3+3]-type $\mathbf{1b}_3{\cdot}Zn^{II}_3$ as the major species along with [2+2]-type $\mathbf{1b}_2{\cdot}Zn^{II}_2$ (minor species) due to the restriction around Zn^{II} by the α-methyl substituents. Isolations of both $\mathbf{1b}_2{\cdot}Zn^{II}_2$ and $\mathbf{1b}_3{\cdot}Zn^{II}_3$ were achieved by gel permeation chromatography (GPC). Similar to $\mathbf{1a}_2{\cdot}Zn^{II}_2$, the ^{1}H NMR spectra of $\mathbf{1b}_2{\cdot}Zn^{II}_2$ and $\mathbf{1b}_3{\cdot}Zn^{II}_3$ also suggested fast changes in the relative orientations at the Zn^{II} complexing moieties (Figure 2b). $\mathbf{1b}_2{\cdot}Zn^{II}_2$ exhibited ^{1}H NMR signals at $\delta = 6.46/5.92$ and 1.95 ppm for pyrrole β-H and α-methyl units, respectively, whereas $\mathbf{1b}_3{\cdot}Zn^{II}_3$ showed the corresponding signals at $\delta = 6.57/6.18$ and 2.09 ppm, respectively. The upfield-shifted signals of $\mathbf{1b}_2{\cdot}Zn^{II}_2$ may be ascribable to the distorted geometry that results in the shielding effect of the π-conjugated aromatic moieties being directed to the opposite side. The relative stability per $\mathbf{1a}{\cdot}Zn^{II}$ moiety of $\mathbf{1b}_3{\cdot}Zn^{II}_3$ compared with $\mathbf{1b}_2{\cdot}Zn^{II}_2$ at the B3LYP/6–31G(d,p) level is 0.98 kcal mol^{-1}.[5] From the experimental and theoretical observations, it is difficult to discuss the relationship between the relative stabilities of cyclic oligomers and the isolated yields. The introduction of methyl groups at dipyrrin α-positions was found to control the stable polygon-like Zn^{II}-bridged assemblies. Furthermore, the UV/Vis absorption spectra of $\mathbf{1a}_2{\cdot}Zn^{II}_2$, $\mathbf{1b}_2{\cdot}Zn^{II}_2$, and $\mathbf{1b}_3{\cdot}Zn^{II}_3$ in CH_2Cl_2 exhibited absorption bands with maxima at 504, 514, and 492 nm, respectively, which were redshifted compared with those of metal-free **1a**,**b** at 436 and 447 nm. The high molar coefficient (ε) at the redshifted region in $\mathbf{1b}_3{\cdot}Zn^{II}_3$ ($2.0\times10^5\,M^{-1}cm^{-1}$ at 492 nm) is often observed in the Zn^{II} complex of dipyrrin possessing α-methyl substituents, $\mathbf{3}_2{\cdot}Zn^{II}$, exhibiting absorption at 491 nm ($\varepsilon = 1.3\times10^5\,M^{-1}cm^{-1}$), whereas $\mathbf{1b}_2{\cdot}Zn^{II}_2$ showed smaller ε possibly due to the distorted coordination geometries.

Single-crystal X-ray structures of $\mathbf{1a}_2{\cdot}Zn^{II}_2$ and $\mathbf{1b}_3{\cdot}Zn^{II}_3$ revealed the exact geometries of the cyclic complexes and their packing structures (Figure 3). The solid-state structure of $\mathbf{1a}_2{\cdot}Zn^{II}_2$ shows the ellipse-like [2+2]-type assembly with distortions around the Zn^{II} complex units and ethynyl moieties: the dihedral angles between them are 80.2 and 85.7° (two independent structures) and the intramolecular Zn···Zn distances are 7.34 and 7.65 Å (Figure 3a(i)). These independent Zn^{II}-bridged macrocycles are arranged in the different layers in parallel orientation (Figure 3a(ii)). Each macrocycle forms an intermolecular C–H···π interaction between the dipyrrins and spacer phenyl moieties in different fashions. The solid-state structures of $\mathbf{1a}_2{\cdot}Zn^{II}_2$, whose con-

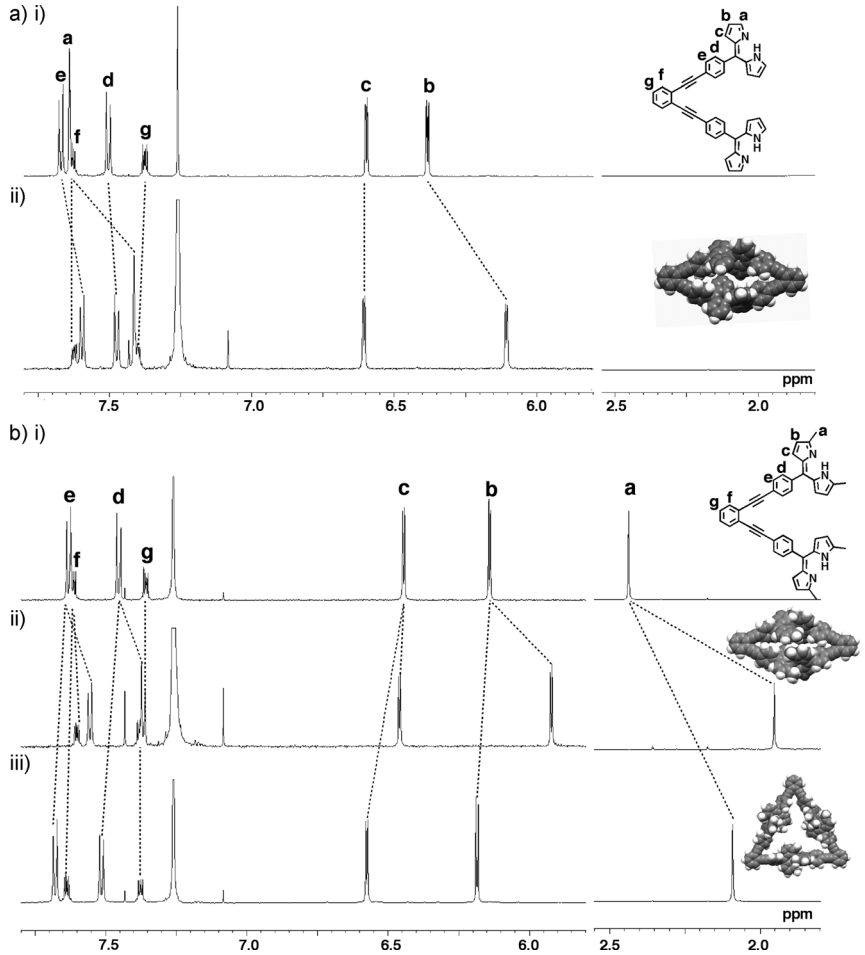

Figure 2. ^{1}H NMR spectra of a) i) **1a** and ii) **1a**$_2$·Zn$^{II}_2$ and b) i) **1b**, ii) **1b**$_2$·Zn$^{II}_2$, and iii) **1b**$_3$·Zn$^{II}_3$ in $CDCl_3$ and DFT-optimized model structures of metal-bridged macrocycles.

stituting dipyrrin planes were almost parallel and perpendicular to the macrocycle plane, were in contrast to the DFT-optimized structure (inset of Figure 2a(ii)). On the other hand, **1b**$_3$·Zn$^{II}_3$ forms a triangular [3+3]-type complex (Figure 3b(i)), which has three sides (labeled as A–C) possessing different distorted metal-complexing structures, and **1b**$_3$·Zn$^{II}_3$ forms the packing structure by using intermolecular interactions between the same sides in the neighboring complexes (Figure 3b(ii)). Fairly planar 1D structures are fabricated by the C–H···π interactions between the two sides A and the two sides B. Furthermore, intermolecular C–H···π interactions between the dipyrrin moieties and intermolecular π–π interactions between the dipyrrins and the phenyl moieties (π···π distance: 3.57 Å) at the sides C provide step-like 2D structures based on the 1D structures. The distorted triangle structure of the solid-state **1b**$_3$·Zn$^{II}_3$ was quite different from the DFT-optimized fairly symmetrical triangle (inset of Figure 2b(iii)). As an essential point for the electronic properties in the bulk materials, it is noteworthy that **1b**$_3$·Zn$^{II}_3$ shows the proximal arrangement of constituting π-conjugated moieties in the solid state, in contrast to **1a**$_2$·Zn$^{II}_2$, which locates π units with longer distances.

It is significant to exhibit the metal complexation behaviors for other metal cations to show the possibility to provide a variety of metal-bridged macrocycles based on the pyrrole-based π-conjugated ligand molecules. Acyclic ligands such as dipyrrins can form various metal-coordination modes depending on the metal cations. In fact, cyclization by metal ions that prefer square-planar coordination geometries, such as Ni^{II}, was examined. Ni^{II} complexation of **1a**,**b** also resulted in the formation of **1a**$_2$·Ni$^{II}_2$, **1b**$_2$·Ni$^{II}_2$, and **1b**$_3$·Ni$^{II}_3$ (Figure 1 bottom) as seen in Table 1 for the yields. As observed in the Ni^{II} complexes of dipyrrins,[6] the ^{1}H NMR spectra of these Ni^{II} complexes showed paramagnetic behaviors, exhibiting signals over a wide range due to distortion from the diamagnetic Ni^{II} square-planar structure. In particular, α-methyl-substituted **1b**$_2$·Ni$^{II}_2$ and **1b**$_3$·Ni$^{II}_3$ showed signals from $\delta = 65$ to -10 ppm. A similar trend was also observed in the mononuclear Ni^{II} complex of dipyrrin possessing α-methyl substituents, **3**$_2$·Ni^{II}. The optimized structures of **1a**$_n$·Ni$^{II}_n$ and **1b**$_n$·Ni$^{II}_n$ ($n = 2, 3$) at the PM6 level showed distortions of the Ni^{II}-bridged dipyrrin–dipyrrin dihedral angles of 64.5, 66.2, and 60.5° in **1a**$_2$·Ni$^{II}_2$, **1b**$_2$·Ni$^{II}_2$, and **1b**$_3$·Ni$^{II}_3$, respectively.[5] The optimized structure of **1b**$_2$·Ni$^{II}_2$ showed a larger distortion than that of **1a**$_2$·Ni$^{II}_2$ due to the steric hindrance of the α-substituents, resulting in the paramagnetic behavior of **1b**$_2$·Ni$^{II}_2$.

Hexadecyloxy-substituted dipyrrin dimers **2a**,**b**, possessing long alkyl chains in the spacer moieties, also provided metal (Zn^{II} and Ni^{II}) complexes: **2a**$_n$·Zn$^{II}_n$, **2b**$_n$·Zn$^{II}_n$, **2a**$_n$·Ni$^{II}_n$, and **2b**$_n$·Ni$^{II}_n$ ($n = 2, 3$; Figure 1 bottom, Table 1). Fascinatingly, transformations between **2a**$_2$·Zn$^{II}_2$ and **2a**$_3$·Zn$^{II}_3$ were observed in $CDCl_3$ solution (**2a**$_2$·Zn$^{II}_2$ ← **2a**$_3$·Zn$^{II}_3$) and by removal of the solvent (**2a**$_2$·Zn$^{II}_2$ → **2a**$_3$·Zn$^{II}_3$), whereas [2+2]-type **2b**$_2$·Zn$^{II}_2$ and [3+3]-type **2b**$_3$·Zn$^{II}_3$ were isolated by GPC-HPLC. The ^{1}H NMR integrals had a ratio of 2:1 immediately after solubilizing the mixture of **2a**$_2$·Zn$^{II}_2$ and **2a**$_3$·Zn$^{II}_3$ in $CDCl_3$, along with higher oligomers as minor species, and it changed to 5:1 after 10 h and returned to 2:1 after the removal of the solvent. A more detailed investigation is required, but the long alkyl chains in **2a**$_n$·Zn$^{II}_n$ may influence the stable states, which are different in solution

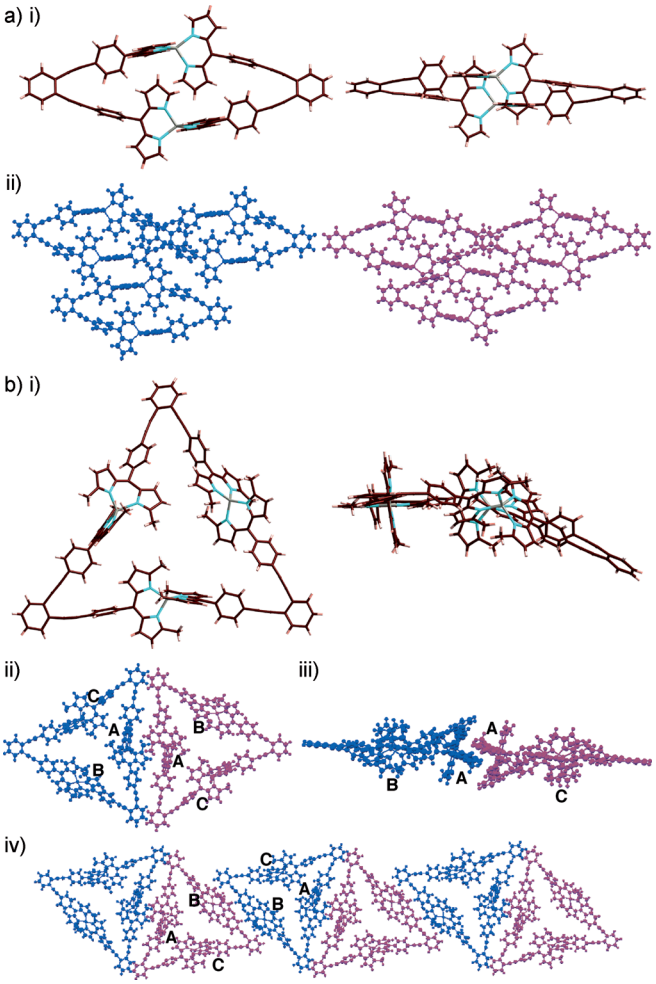

Figure 3. Single-crystal X-ray structures of a) $\mathbf{1a}_2{\cdot}Zn^{II}_2$ as i) a monomer structure (top and side view) of the two independent structures and ii) two kinds of packing diagram, wherein the molecules in different colors are independent structures in the different layers and b) $\mathbf{1b}_3{\cdot}Zn^{II}_3$ as i) a monomer structure (top and side view) and ii)–iv) packing diagrams, wherein the molecules in different colors are identical but arranged in different orientations in the packing diagrams. Atom color code for a) i) and b) i): brown, pink, blue, and magenta indicate carbon, hydrogen, nitrogen, and zinc, respectively. The labels A, B, and C denote the different sides of the triangular [3+3]-type complex.

and solid state. On the other hand, the lack of transition between $\mathbf{2b}_2{\cdot}Zn^{II}_2$ and $\mathbf{2b}_3{\cdot}Zn^{II}_3$ in $CDCl_3$ is ascribable to the protecting behaviors of α-methyl moieties around the metal complexation units. This observation suggests that α-methyl substituents affected not only the geometries of the *meta*-bridged macrocycles but also the stabilities of the cyclic structures.[7] A similar trend was observed in the Ni^{II} complexes of **2a**,**b**. Ni^{II} complexation of **2a** showed multiple complexes, which could not be isolated, whereas **2b** provided $\mathbf{2b}_2{\cdot}Ni^{II}_2$ and $\mathbf{2b}_3{\cdot}Ni^{II}_3$, which were separated by GPC-HPLC and showed magnetic properties like those of $\mathbf{1b}_n{\cdot}Ni^{II}_n$ ($n=2$, 3).

The small π–π distances aligned in 1D fashion with the step-like 2D network structure are expected to provide highly electrically conductive pathways for charge carriers, especially in the crystalline state of triangular $\mathbf{1b}_3{\cdot}Zn^{II}_3$. The presence of the pathways was examined by non-contact flash-photolysis time-resolved microwave conductivity (FP-TRMC) measurement in the polycrystalline solid films of $\mathbf{1a}_2{\cdot}Zn^{II}_2$ and $\mathbf{1b}_3{\cdot}Zn^{II}_3$ (Figure 4a).[8] Clear conductivity transients were observed for both compounds in polycrystalline state with extremely long lifetimes exceeding 50 μs.

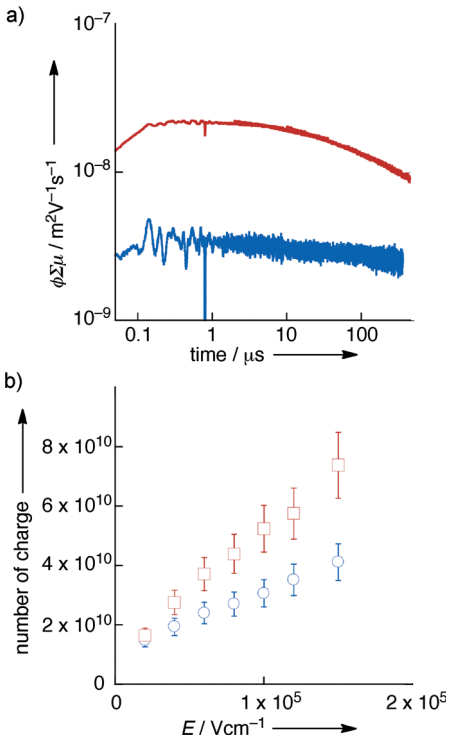

Figure 4. a) TRMC transients observed for polycrystalline $\mathbf{1a}_2{\cdot}Zn^{II}_2$ (blue) and $\mathbf{1b}_3{\cdot}Zn^{II}_3$ (red) over a wide range after 355 nm pulse excitation and b) the dependence of increasing numbers of photo-carriers for $\mathbf{1a}_2{\cdot}Zn^{II}_2$ (blue) and $\mathbf{1b}_3{\cdot}Zn^{II}_3$ (red) with the electric field strength applied to electrodes. The yield of photo-carrier injection was estimated by the extrapolation of the dependence at $E=0$, the identical field strength for TRMC measurement ($E\approx10^1$ Vcm^{-1}).

Almost identical kinetic traces were observed under O_2-saturated conditions with a slightly higher yield of photo-carrier injection, suggesting that positive holes are the major carrier species, and triplet excited states with high transient complex dielectric constants provide negligible contributions to the conductivity transients. The minimum limit mobilities of holes, of $(1.4\pm0.4)\times10^{-2}$ $cm^2V^{-1}s^{-1}$ in $\mathbf{1a}_2{\cdot}Zn^{II}_2$ and (0.11 ± 0.03) $cm^2V^{-1}s^{-1}$ in $\mathbf{1b}_3{\cdot}Zn^{II}_3$, were deduced from the yields of photo-carrier injections determined by photo-current measurement as $\phi=(2.4\pm0.5)\times10^{-3}$ for $\mathbf{1a}_2{\cdot}Zn^{II}_2$ and $(2.1\pm0.5)\times10^{-3}$ for $\mathbf{1b}_3{\cdot}Zn^{II}_3$ (Figure 4b).[9] The mobility in $\mathbf{1b}_3{\cdot}Zn^{II}_3$ approaches the cross-over range of hopping and band conduction mechanisms of charge carriers. The well-aligned π-electron systems and the small contact distances reduce hopping barriers for holes in $\mathbf{1b}_3{\cdot}Zn^{II}_3$ arrays. A photo-conductivity transient was also observed for the

simple dispersive system of $\mathbf{1b}_3{\cdot}Zn^{II}_3$ in a polystyrene matrix (the Supporting Information, Figure S24), showing considerable breakdown of conductive pathways in the system. This also supports that the well-aligned π-electron systems and the small contact distances reduce hopping barriers for holes in $\mathbf{1b}_3{\cdot}Zn^{II}_3$ arrays. This explains why the hole mobility observed in the triangular $\mathbf{1b}_3{\cdot}Zn^{II}_3$ is higher than that in ellipsoidal $\mathbf{1a}_2{\cdot}Zn^{II}_2$ by one order of magnitude. On the other hand, the metal complex $\mathbf{2b}_3{\cdot}Zn^{II}_3$, possessing long alkyl chains, showed less-effective electric conductivity.

Conclusion

Polygon-like [2+2]- and [3+3]-type metal-bridged assemblies based on dipyrrin moieties were fabricated. The electrical conduction depends strongly on the packing alignment of the compounds, revealing the presence of effective hopping pathways for holes with relatively high mobility up to 0.11 $cm^2V^{-1}s^{-1}$ along the aligned axis of [3+3]-type metal-bridged assemblies. These observations were significantly correlated with the geometrical control of the π-conjugated metal complexes in the cyclic structures, which enables their ordered arrangement in the assemblies. Modification of π-conjugated units in the metal ligand and spacer units could yield fascinating metal complexes and assemblies, and their preparations are currently underway.

Experimental Section

General procedures: Starting materials were purchased from Wako Pure Chemical Industries Ltd., Nacalai Tesque Inc., and Sigma–Aldrich Co. and used without further purification unless otherwise stated. UV/Visible spectra were recorded on a Hitachi U-3500 spectrometer. Fluorescence spectra were recorded on a Hitachi F-4500 fluorescence spectrometer. NMR spectra used in the characterization of products were recorded on a JEOL ECA-600 600 MHz spectrometer. All NMR spectra were referenced to solvent. Matrix-assisted laser desorption ionization time-of-flight mass spectrometries (MALDI-TOF-MS) were recorded on a Shimadzu Axima-CFRplus using negative mode. Fourier transform ion cyclotron resonance mass spectrometries (FT-ICR-MS) were recorded on a Bruker solariX (Qh-FT-ICR-MS) and were carried out in the Joint Usage/Research Center (JURC) at Institute for Chemical Research (ICR), Kyoto University with the help of Prof. Hikaru Takaya and Dr. Katsuhiro Isozaki, Kyoto University. Elemental analyses were performed on a Yanaco CHN corder MT series for carbon, hydrogen, and nitrogen, the Laboratory for Organic Elemental Microanalysis, Kyoto University. TLC analyses were carried out on aluminum sheets coated with silica gel 60 (Merck 5554). Column chromatography was performed on Sumitomo alumina KCG-1525, Wakogel C-200, C-300, Merck silica gel 60 and 60 H, and Bio-Beads S-X1 Beads (for gel permeation chromatography (GPC)). GPC-HPLC was performed on a JAI LC-9225 with JAIGEL-2H and JAIGEL-2.5H columns.

1,2-Di(4-formylphenylethynyl)benzene (s1): Following the literature procedure,[4a,b] a mixture of 4-bromobenzaldehyde (3.376 g, 18.3 mmol), 1,2-diethynylbenzene (0.929 g, 7.3 mmol), triethylamine (1.52 mL, 10.9 mmol), $[Pd(PPh_3)_2Cl_2]$ (153.7 mg, 0.22 mmol), PPh_3 (24.6 mg, 0.094 mmol), and CuI (69.5 mg, 0.36 mmol) in THF (67 mL) was heated at reflux under nitrogen for 26 h. The reaction mixture was diluted with CH_2Cl_2 (100 mL), washed with saturated aqueous NH_4Cl (50 mL) and brine (50 mL), and then dried over $MgSO_4$ and evaporated. The residue was purified by silica gel column chromatography (Wakogel C-300; CH_2Cl_2/*n*-hexane = 6/1) and recrystallized from CH_2Cl_2/*n*-hexane to afford **s1** as a yellow solid (1.12 g, 3.34 mmol, 46%). R_f = 0.33 (CH_2Cl_2); ^{1}H NMR (600 MHz, $CDCl_3$, 20 °C): δ = 10.03 (s, 2H; CHO), 7.89 (d, *J* = 8.4 Hz, 4H; Ar-H), 7.71 (d, *J* = 8.4 Hz, 2H; Ar-H), 7.62 (dd, *J* = 5.4, 3.6 Hz, 4H; Ar-H), 7.41 ppm (dd, *J* = 5.4, 3.6 Hz, 2H; Ar-H); MALDI-TOF-MS: *m*/*z* (%): calcd for $C_{24}H_{14}O_2$: 334.10 $[M]^-$; found 335.0 (100), 336.0 (26).

1,2-Bis(4-dipyrrolylmethylphenylethynyl)benzene (s2a): TFA (0.014 mL, 0.20 mmol) was added to aldehyde **s1** (219 mg, 0.65 mmol) dissolved in pyrrole (10 mL) after being degassed by bubbling with nitrogen for 10 min. After the solution was stirred for 10 min, triethylamine (1 mL) was added. The solution was removed by vacuum distillation with gentle heating. The residue was chromatographed over flash silica gel column (CH_2Cl_2/*n*-hexane = 5:1) to give **s2a** as a yellow solid (224.5 mg, 0.40 mmol, 61%). R_f = 0.35 (CH_2Cl_2); ^{1}H NMR (600 MHz, $CDCl_3$, 20 °C): δ = 7.95 (br s, 4H; NH), 7.56 (dd, *J* = 6.0, 3.6 Hz, 2H; Ar-H), 7.51 (d, *J* = 8.4 Hz, 4H; Ar-H), 7.32 (dd, *J* = 6.0, 3.6 Hz, 2H; Ar-H), 7.23 (d, *J* = 8.4 Hz, 4H; Ar-H), 6.72 (m, 4H; pyrrole-H), 6.17 (m, 4H; pyrrole-H), 5.91 (br, 4H; pyrrole-H), 5.49 ppm (s, 2H; *meso*-H); MALDI-TOF-MS: *m*/*z* (%): calcd for $C_{40}H_{30}N_4$: 566.25 $[M]^-$; found 566.3 (100), 567.3 (34).

1,2-Bis[4-di(5-methylpyrrol-2-yl)methylphenylethynyl]benzene (s2b): TFA (0.023 mL, 0.30 mmol) was added to aldehyde **s1** (334 mg, 1.00 mmol) and 2-methylpyrrole (405 mg, 5.0 mmol) dissolved in CH_2Cl_2 (80 mL). After the solution was stirred for 10 min, triethylamine (1 mL) was added and the solution was evaporated. The residue was purified by silica gel column chromatography (Wakogel C-300; CH_2Cl_2) to give **s2b** as a yellow solid (431 mg, 0.69 mmol, 69%). R_f = 0.33 (CH_2Cl_2); ^{1}H NMR (600 MHz, $CDCl_3$, 20 °C): δ = 7.65 (br s, 4H; NH), 7.56 (dd, *J* = 6.0, 3.6 Hz, 2H; Ar-H), 7.51 (d, *J* = 8.4 Hz, 4H; Ar-H), 7.31 (dd, *J* = 6.0, 3.0 Hz, 2H; Ar-H), 7.23 (d, *J* = 8.4 Hz, 4H; Ar-H), 5.80 (m, 4H; pyrrole-H), 5.75 (m, 4H; pyrrole-H), 5.38 (s, 2H; *meso*-H), 2.22 ppm (s, 12H; α-Me); MALDI-TOF-MS: *m*/*z* (%): calcd for $C_{44}H_{38}N_4$: 622.31 $[M]^+$; found 622.4 (100), 623.4 (58).

1,2-Bis(4-dipyrrilylphenylethynyl)benzene (1a): Dipyrromethane **s2a** (46.1 mg, 0.081 mmol) was dissolved in THF (30 mL) and stirred in an ice bath. 2,3-Dichloro-5,6-dicyanobenzoquinone (DDQ; 40.5 mg, 0.178 mmol) in THF (30 mL) was added slowly dropwise over the course of 70 min. DDQ was removed by alumina column and the solution was evaporated. The residue was purified by silica gel column chromatography (Wakogel C-300; 3% MeOH/CH_2Cl_2) to afford **1a** as a yellow film (22.7 mg, 0.04 mmol, 49%). R_f = 0.35 (3% MeOH/CH_2Cl_2); ^{1}H NMR (600 MHz, $CDCl_3$, 20 °C; see also the Supporting Information, Figure S1): δ = 7.68 (d, *J* = 8.4 Hz, 4H; Ar-H), 7.66–7.61 (m, 6H; pyrrole-H and Ar-H), 7.51 (d, *J* = 8.4 Hz, 4H; Ar-H), 7.39 (dd, *J* = 6.0, 3.6 Hz, 2H; Ar-H), 6.60 (m, 4H; pyrrole-H), 6.39 ppm (m, 4H; pyrrole-H); UV/Vis (CH_2Cl_2): λ_{max} (ε) = 435.5 nm (3.9×10^4 $M^{-1}cm^{-1}$); MALDI-TOF-MS: *m*/*z* (%): calcd for $C_{40}H_{26}N_4$: 562.22 $[M]^+$; found 562.7 (100), 563.7 (70).

1,2-Bis[4-(5,5′-dimethyldipyrrilyl)phenylethynyl]benzene (1b): Dipyrromethane **s2b** (431 mg, 0.69 mmol) was dissolved in THF (60 mL) and stirred in an ice bath. DDQ (343.05 mg, 1.51 mmol) in THF (60 mL) was added slowly dropwise over the course of 80 min. DDQ was removed by alumina column and the solution was evaporated. The residue was purified by flash silica gel column chromatography (2% MeOH/CH_2Cl_2) to afford **1b** as a dark yellow solid (242 mg, 0.39 mmol, 57%). R_f = 0.35 (9% MeOH/CH_2Cl_2); ^{1}H NMR (600 MHz, $CDCl_3$, 20 °C; see also the Supporting Information, Figure S2): δ = 7.63–7.61 (m, 6H; Ar-H and pyrrole-H), 7.46 (d, *J* = 8.4 Hz, 4H; Ar-H), 7.36 (dd, *J* = 5.4, 3.6 Hz, 2H; Ar-H), 6.45 (d, *J* = 4.2 Hz, 4H; pyrrole-H), 6.14 (d, *J* = 4.2 Hz, 4H; pyrrole-H), 2.44 ppm (s, 12H; α-Me); UV/Vis (CH_2Cl_2): λ_{max} (ε) = 447.0 nm (5.4×10 $M^{-1}cm^{-1}$); MALDI-TOF-MS: *m*/*z* (%): calcd for $C_{44}H_{34}N_4$: 618.77 $[M]^+$; found: 618.6 (100), 619.6 (61), 620.6 (20).

[2+2]-Type Zn^{II} complex of 1a, $\mathbf{1a}_2{\cdot}Zn^{II}_2$: Dipyrrin **1a** (10.12 mg, 0.018 mmol) in THF (3 mL) was added to $Zn(OAc)_2{\cdot}2H_2O$ (3.95 mg, 0.018 mmol) in THF (3 mL) and the solution was stirred for 8 h. After this time, an orange precipitate was formed. The precipitate was filtered and recrystallized from CH_2Cl_2/*n*-hexane to afford $\mathbf{1a}_2{\cdot}Zn^{II}_2$ as an orange solid (6.7 mg, 0.011 mmol, 60%). R_f = 0.40 (3% MeOH/CH_2Cl_2); m.p.

>300 °C; ^{1}H NMR (600 MHz, $CDCl_3$, 20 °C; see also the Supporting Information, Figure S3): δ=7.63 (dd, J=3.6, 1.8 Hz, 4H; Ar-H), 7.60 (d, J=8.4 Hz, 8H; Ar-H), 7.48 (d, J=8.4 Hz, 8H; Ar-H), 7.41–7.39 (m, 12H; Ar-H and pyrrole-H), 6.61 (d, J=4.2 Hz, 8H; pyrrole-H), 6.11 ppm (dd, J=3.0, 1.2 Hz, 8H; pyrrole-H); UV/Vis (CH_2Cl_2): λ_{max} (ε)=504.5 nm (12×10^4 M^{-1}cm^{-1}); ESI-TOF-MS (observed in the presence of $AgClO_4$): m/z (%): calcd for $C_{80}H_{48}N_8Zn_2$•Ag: 1355.16 [M+Ag]$^+$; found 1355.16 (8), 1356.16 (31), 1357.17 (82), 135817 (71), 1359.17 (100), 1660.17 (78), 1361.16 (81), 1362.17 (54), 1363.17 (43), 1364.17 (27), 1365.17 (19), 1366.17 (9); elemental analysis calcd (%) for $C_{80}H_{48}N_8Zn_2$·2H_2O: C 74.60, H 4.07, N 8.70; found: C 74.65, H 3.92, N 8.69. This compound was characterized by single-crystal X-ray diffraction analysis.

[n+n]-Type Zn^{II} complexes of 1a, 1a$_n$•Zn$^{II}_n$: Another procedure using diluted condition compared to the reaction for **1a**$_2$·Zn$^{II}_2$ provided the mixture of various complexes **1a**$_n$•Zn$^{II}_n$. Zn(OAc)$_2$•2H_2O (2.63 mg, 0.012 mmol) in THF (20 mL) was added to dipyrrin **1a** (6.74 mg, 0.012 mmol) in THF (20 mL) and the solution was stirred for 4 h. After this time, the reaction solution was diluted with CH_2Cl_2 (100 mL), washed with saturated aqueous Na_2CO_3 (30 mL) and brine (30 mL), and then dried over $MgSO_4$ and evaporated to afford **1a**$_n$•Zn$^{II}_n$ (mixture) as an orange solid. See the details in the ^{1}H NMR spectra (600 MHz, $CDCl_3$, 20 °C) and FT-ICR-MS (the Supporting Information, Figure S4).

[2+2]-Type Zn^{II} complex of 1b, 1b$_2$•Zn$^{II}_2$: Zn(OAc)$_2$•2H_2O (16.94 mg, 0.08 mmol) was added to dipyrrin **1b** (49.5 mg, 0.08 mmol) in THF (26 mL) and the solution was stirred for 3 h. After this time, the reaction mixture was purified by GPC column with THF and recrystallized from $CHCl_3$/n-hexane to afford **1b**$_2$•Zn$^{II}_2$ as an orange solid (7.5 mg, 0.005 mmol, 13%). R_f=0.50 (CH_2Cl_2/n-hexane=1:1); m.p.>300 °C (decomp); ^{1}H NMR (600 MHz, $CDCl_3$, 20 °C; see also the Supporting Information, Figure S5): δ=7.61 (dd, J=6.0, 3.0 Hz, 4H; Ar-H), 7.56 (d, J=7.2 Hz, 8H; Ar-H), 7.39–7.36 (m, 12H; Ar-H and pyrrole-H), 6.46 (d, J=4.2 Hz, 8H; pyrrole-H), 5.92 (d, J=4.2 Hz, 8H; pyrrole-H), 1.95 ppm (s, 24H; α-Me); UV/Vis (CH_2Cl_2): λ_{max} (ε)=513.5 nm (8.9×10^4 M^{-1}cm^{-1}); FT-ICR-MS (MALDI): m/z (%): calcd for $C_{88}H_{64}N_8Zn_2$: 1360.38 [M]$^+$; found 1360.4 (58), 1361.4 (66), 1363.4 (100), 1364.4 (98), 1365.4 (96), 1366.4 (64), 1367.4 (56), 1368.4 (31), 1369.4 (16); elemental analysis calcd (%) for $C_{88}H_{64}N_8Zn_2$·H_2O: C 76.46, H 4.81, N 8.11; found: C 76.90, H 4.88, N 7.62.

[3+3]-Type Zn^{II} complex of 1b, 1b$_3$•Zn$^{II}_3$: Zn(OAc)$_2$•2H_2O (16.94 mg, 0.08 mmol) was added to dipyrrin **1b** (49.5 mg, 0.08 mmol) in THF (26 mL) and the solution was stirred for 3 h. After this time, the reaction mixture was purified by GPC column with THF and recrystallized from $CHCl_3$/hexane to afford **1b**$_3$•Zn$^{II}_3$ as an orange solid (13.4 mg, 0.006 mmol, 24%). R_f=0.43 (CH_2Cl_2/n-hexane=1:1); m.p.>300 °C (decomp); ^{1}H NMR (600 MHz, $CDCl_3$, 20 °C; see also the Supporting Information, Figure S6): δ=7.68 (d, J=8.4 Hz, 12H; Ar-H), 7.64 (dd, J=6.0, 3.6 Hz, 6H; Ar-H), 7.52 (d, J=8.4 Hz, 12H; Ar-H), 7.38 (dd, J=6.0, 3.0 Hz, 6H; Ar-H), 6.57 (d, J=4.2 Hz, 12H; pyrrole-H), 6.18 (d, J=4.2 Hz, 12H; pyrrole-H), 2.09 ppm (s, 36H; α-Me); UV/Vis (CH_2Cl_2): λ_{max} (ε)=492.0 nm (1.9×10^4 M^{-1}cm^{-1}); ESI-TOF-MS (observed in the presence of $AgClO_4$): m/z (%): calcd for $C_{132}H_{96}N_{12}Zn_3$·Ag: 2147.48 [M+Ag]$^+$; found 2147.50 (20), 2148.49 (24), 2149.48 (44), 2150.49 (57), 2151.49 (80), 2152.47 (85), 2153.48 (95), 2154.48 (100), 2155.49 (88), 2156.50 (71), 2157.47 (57), 2158.48 (44), 2159.49 (28), 2160.49 (22), 2161.50 (14); elemental analysis calcd (%) for $C_{132}H_{96}N_{12}Zn_3$: C 77.47, H 4.73, N 8.21; found: C 76.96, H 4.57, N 8.12. This compound was characterized by using single-crystal X-ray diffraction analysis.

[2+2]-Type Ni^{II} complex of 1a, 1a$_2$•Ni$^{II}_2$: Dipyrrin **1a** (42.8 mg, 0.076 mmol) in THF (10 mL) was added to a solution of Ni(OAc)$_2$•4H_2O (19.3 mg, 0.076 mmol) in THF (10 mL), and the solution was stirred for 6 h. The reaction mixture was diluted with CH_2Cl_2 (30 mL), washed with saturated aqueous Na_2CO_3 (30 mL) and brine (30 mL), and then dried over $MgSO_4$ and evaporated. The residue was recrystallized from CH_2Cl_2/n-hexane to afford **1a**$_2$•Ni$^{II}_2$ as a red solid (33.2 mg, 0.027 mmol, 72%). R_f=0.43 (3% MeOH/CH_2Cl_2); m.p.>300 °C (decomp); ^{1}H NMR (600 MHz, CD_2Cl_2, 0 °C; two kinds of protons are missing presumably due to the overlap with other protons: see also the Supporting Information, Figure S7): δ=10.65 (brs, 4H; pyrrole-H), 8.60 (brs, 4H; pyrrole-H), 8.06 (brs, 4H; pyrrole-H), 7.65–7.63 (m, 6H; Ar-H), 7.56 (m, 2H; Ar-H), 7.47–7.38 (m, 12H; Ar-H), 7.22 (d, J=7.8 Hz, 4H; Ar-H), 7.11 (brs, 4H; pyrrole-H), 6.79 (d, J=4.2 Hz, 4H; pyrrole-H), 6.75 ppm (d, J=4.2 Hz, 4H; pyrrole-H); UV/Vis (CH_2Cl_2): λ_{max} (ε)=477.0 nm (5.7×10^4 M^{-1}cm^{-1}); ESI-TOF-MS (observed in the presence of $AgClO_4$): m/z (%): calcd for $C_{80}H_{48}N_8Ni_2$·Ag: 1343.18 [M]$^+$; found 1343.18 (48), 1344.19 (44), 1345.18 (100), 1346.18 (81), 1347.18 (78), 1348. 18 (53), 1349. 18 (38), 1350.18 (27), 1351.18 (16); elemental analysis calcd (%) for $C_{80}H_{48}N_8Ni_2$: C 77.57, H 3.91, N 9.05; found: C 76.81, H 3.80, N 8.81.

[2+2]-Type of Ni^{II} complex of 1b, 1b$_2$•Ni$^{II}_2$: Ni(OAc)$_2$•4H_2O (10.45 mg, 0.042 mmol) was added to dipyrrin **1b** (26.05 mg, 0.042 mmol) in THF (14 mL) and the solution was stirred for 4 h. After this time, the reaction mixture was diluted with CH_2Cl_2 (30 mL), washed with saturated aqueous Na_2CO_3 (30 mL) and brine (30 mL), and then dried over $MgSO_4$ and evaporated. The residue was purified by GPC column with THF to give **1b**$_2$•Ni$^{II}_2$ as a red solid (2.5 mg, 0.002 mmol, 9.5%). R_f=0.36 (CH_2Cl_2/n-hexane=1/1); m.p.>300 °C (decomp); ^{1}H NMR (600 MHz, $CDCl_3$, 20 °C; see also the Supporting Information, Figure S8): δ=64.75 (s, 8H; pyrrole-H), 42.04 (s, 24H; CH_3), 6.48 (d, J=7.8 Hz, 4H; Ar-H), 6.30 (d, J=9.6 Hz, 4H; Ar-H), 3.59 (s, 8H; Ar-H), 0.16 (s, 8H; Ar-H), −10.51 ppm (s, 8H; pyrrole-H); UV/Vis (CH_2Cl_2): λ_{max} (ε)=516.5 nm (6.3×10^4 M^{-1}cm^{-1}); FT-ICR-MS (MALDI): m/z (%): calcd for $C_{88}H_{64}N_8Ni_2$: 1348.40 [M]$^+$; found: 1348.4 (84), 1349.4 (100), 1350.4 (95), 1351.4 (93), 1352.4 (65), 1353.4 (42), 1354.4 (23), 1355.4 (12), 1356.4 (43), 1357.4 (5); elemental analysis calcd (%) for $C_{88}H_{64}N_8Ni_2$·4H_2O: C 74.28, H 5.10, N 7.87; found: C 74.16, H 5.30, N 7.32.

[3+3]-Type Ni^{II} complex of 1b, 1b$_3$•Ni$^{II}_3$: Ni(OAc)$_2$•4H_2O (10.45 mg, 0.042 mmol) was added to dipyrrin **1b** (26.05 mg, 0.042 mmol) in THF (14 mL) and the solution was stirred for 4 h. After this time, the reaction mixture was diluted with CH_2Cl_2 (30 mL), washed with saturated aqueous Na_2CO_3 (30 mL) and brine (30 mL), and then dried over $MgSO_4$ and evaporated. The residue was purified by GPC column with THF to give **1b**$_3$•Ni$^{II}_3$ as a red solid (9.3 mg, 0.005 mmol, 32%). R_f=0.42 (CH_2Cl_2/n-hexane=1:1); m.p.>300 °C (decomp); ^{1}H NMR (600 MHz, $CDCl_3$, 20 °C; see also the Supporting Information, Figure S9): δ=63.68 (s, 12H; pyrrole-H), 41.14 (s, 36H; CH_3), 6.40 (s, 6H; Ar-H), 6.18 (s, 6H; Ar-H), 3.34 (s, 12H; Ar-H), 0.71 (s, 12H; Ar-H), −10.28 ppm (s, 12H; pyrrole-H); UV/Vis (CH_2Cl_2): λ_{max} (ε)=514.5 nm (16×10^4 M^{-1}cm^{-1}); ESI-TOF-MS (observed in the presence of $AgClO_4$): m/z (%): calcd for $C_{132}H_{96}N_{12}Ni_3$•Ag: 2129.50 [M+Ag]$^+$; found: 2129.54 (27), 2130.55 (37), 2131.55 (72), 2132.55 (90), 2133.55 (100), 2134.55 (90), 2135.55 (74), 2136.56 (54), 2137.56 (38), 2138.53 (26), 2139.54 (17); elemental analysis calcd (%) for $C_{132}H_{96}N_{12}Ni_3$·6H_2O: C 74.28, H 5.10, N 7.87; found: C 74.96, H 5.05, N 7.79.

1,2-Dihexadecyloxy-4,5-bis(trimethylsilylethynyl)benzene (s3): TMS-acetylene (2.95 mL, 21.5 mmol) was added to a mixture of 1,2-dihexadecyloxy-4,5-diiodobenzene[10] (6.97 g, 8.6 mmol), [Pd(PPh$_3$)$_2$Cl$_2$] (181 mg, 0.26 mmol), and CuI (81 mg, 0.43 mmol) in THF/triethylamine (40 mL/40 mL) and heated at reflux under nitrogen for 20 h. The reaction mixture was diluted with CH_2Cl_2 (100 mL), washed with saturated aqueous NH_4Cl (50 mL) and brine (50 mL), and then dried over $MgSO_4$ and evaporated. The residue was purified by silica gel column chromatography (Wakogel C-300; $CHCl_3$/n-hexane=1:4) and recrystallized from $CHCl_3$/MeOH to afford **s3** as a white solid (5.99 g, 7.98 mmol, 92%). R_f=0.65 ($CHCl_3$/n-hexane=1/2); ^{1}H NMR (600 MHz, $CDCl_3$, 20 °C): δ=6.89 (s, 2H; Ar-H), 3.96 (t, J=6.6 Hz, 4H; O$CH_2C_{15}H_{31}$), 1.80 (quin, J=6.6 Hz, 4H; OCH$_2$$CH_2C_{14}H_{29}$), 1.39 (m, 4H; OC$_2H_4$$CH_2C_{13}H_{27}$), 1.46–1.15 (m, 48H; OC$_3H_6$$C_{12}H_{24}CH_3$), 0.88 (t, J=6.6 Hz, 6H; OC$_{15}H_{30}$$CH_3$), 0.26 ppm (s, 18H; TMS-H); MALDI-TOF-MS: m/z (%): calcd for $C_{48}H_{86}O_2Si_2$: 750.62 [M]$^-$; found: 750.6 (100), 751.6 (70), 752.6 (30).

4,5-Diethynyl-1,2-dihexadecyloxybenzene (s4): The precursor **s3** (5.99 g, 7.9 mmol) was dissolved in MeOH/THF (60 mL/60 mL) and K_2CO_3 (5.36 g, 39.5 mmol) was added and the solution was stirred at RT. After 4 h, water (150 mL) and $CHCl_3$ (100 mL) were added. Organic phase was separated and water phase was extracted with $CHCl_3$ (30 mL×3). All organic solvents were combined, dried over $MgSO_4$ and evaporated. The residue was purified by silica gel column chromatography (Wakogel C-300; $CHCl_3$/n-hexane=1:7) and recrystallized from $CHCl_3$/MeOH to

afford **s4** as a white solid (4.33 g, 0.90 mmol, 90%). R_f=0.45 ($CHCl_3$/*n*-hexane=1:2); ^{1}H NMR (600 MHz, $CDCl_3$, 20°C): δ=6.95 (s, 2H; Ar-H), 3.98 (t, *J*=6.6 Hz, 4H; O$CH_2C_{15}H_{31}$), 3.25 (s, 2H; ethynyl-H), 1.81 (quin, *J*=6.6 Hz, 4H; $OCH_2CH_2C_{14}H_{29}$), 1.45 (m, 4H; $OC_2H_4CH_2C_{13}H_{27}$), 1.25 (m, 48H; $OC_3H_6C_{12}H_{24}CH_3$), 0.88 ppm (t, *J*=6.6 Hz, 6H, $OC_{15}H_{30}CH_3$); MALDI-TOF-MS: *m*/*z* (%): calcd for $C_{42}H_{70}O_2$: 606.54 $[M]^+$; found 606.6 (100), 607.6 (60), 608.6 (20).

4,5-Di(4-formylphenylethynyl)-1,2-dihexadecyloxybenzene (s5): A mixture of 4-bromobenzaldehyde (3.32 g, 17.9 mmol), compound **s4** (4.33 g, 7.14 mmol), triethylamine (2 mL), $[Pd(PPh_3)_2Cl_2]$ (150.2 mg, 0.21 mmol), PPh_3 (28.9 mg, 0.11 mmol), and CuI (68.0 mg, 0.35 mmol) in THF (66 mL) was heated at reflux under nitrogen for 24 h. The reaction mixture was diluted with CH_2Cl_2 (100 mL), washed with saturated aqueous NH_4Cl (50 mL) and brine (50 mL), and then dried over $MgSO_4$ and evaporated. The residue was purified by silica gel column chromatography (Wakogel C-300; CH_2Cl_2) and recrystallized from $CHCl_3$/MeOH to afford **s5** as a light yellow solid (2.32 g, 2.92 mmol, 41%). R_f=0.33 (CH_2Cl_2); ^{1}H NMR (600 MHz, $CDCl_3$, 20°C): δ=10.02 (s, 2H; CHO), 7.87 (d, *J*=8.4 Hz, 4H; Ar-H), 7.69 (d, *J*=8.4 Hz, 4H; Ar-H), 7.05 (s, 2H; Ar-H), 4.06 (t, *J*=6.6 Hz, 4H; O$CH_2C_{15}H_{31}$), 1.84 (quin, *J*=6.6 Hz, 4H; $OCH_2CH_2C_{14}H_{29}$), 1.46 (m, 4H; $OC_2H_4CH_2C_{13}H_{27}$), 1.37–1.25 (m, 48H; $OC_3H_6C_{12}H_{24}CH_3$), 0.88 ppm (t, *J*=6.6 Hz, 6H; $OC_{15}H_{30}CH_3$); MALDI-TOF-MS: *m*/*z* (%): calcd for $C_{58}H_{78}O_4$: 814.59 $[M]^+$; found: 814.7 (100), 815.8 (60), 816.6 (20).

4,5-Bis(4-dipyrrolylmethylphenylethynyl)-1,2-dihexadecyloxybenzene (s6a): TFA (0.05 mL, 0.36 mmol) was added to aldehyde **s5** (972 mg, 1.2 mmol), which had been dissolved in pyrrole/CH_2Cl_2 (15 mL/25 mL) and degassed by bubbling with nitrogen for 10 min. After the solution was stirred for 15 min, triethylamine (1 mL) was added. The solvent was removed by vacuum distillation with gentle heating. The residue was chromatographed over flash silica gel column (CH_2Cl_2) and recrystallized from $CHCl_3$/MeOH to give **s6a** as a yellow solid (666 mg, 0.64 mmol, 53%). R_f=0.35 (CH_2Cl_2); ^{1}H NMR (600 MHz, $CDCl_3$, 20°C): δ=7.95 (brs, 4H; NH), 7.48 (d, *J*=7.8 Hz, 4H; Ar-H), 7.18 (d, *J*=8.4 Hz, 4H; Ar-H), 7.00 (s, 2H; Ar-H), 6.71 (m, 4H; pyrrole-H), 6.17 (m, 4H; pyrrole-H), 5.91 (br, 4H; pyrrole-H), 5.48 (s, 2H; *meso*-H), 4.03 (t, *J*=6.6 Hz, 4H; O$CH_2C_{15}H_{31}$), 1.85 (quin, *J*=6.6 Hz, 4H; $OCH_2CH_2C_{14}H_{29}$), 1.47 (m, 4H; $OC_2H_4CH_2C_{13}H_{27}$), 1.36–1.21 (m, 48H; $OC_3H_6C_{12}H_{24}CH_3$), 0.88 ppm (t, *J*=6.6 Hz, 6H; $OC_{15}H_{30}CH_3$); MALDI-TOF-MS: *m*/*z* (%): calcd for $C_{72}H_{94}N_4O_2$: 1046.74 $[M]^-$; found: 1046.7 (100), 1047.7 (34), 1048.7 (35).

4,5-Bis(4-di(5-methylpyrrol-2-yl)methylphenylethynyl)-1,2-dihexadecyloxybenzene (s6b): TFA (0.005 mL, 0.07 mmol) was added to aldehyde **s5** (200 mg, 0.25 mmol) and 2-methylpyrrole (101 mg, 1.25 mmol) dissolved in CH_2Cl_2 (20 mL). After the solution was stirred for 15 min, triethylamine (1 mL) was added and the solution was evaporated. The residue was purified by silica gel column chromatography (Wakogel C-300; CH_2Cl_2/*n*-hexane=2/1) to give **s6b** as a yellow solid (162 mg, 0.15 mmol, 59%). R_f=0.58 (CH_2Cl_2); ^{1}H NMR (600 MHz, $CDCl_3$, 20°C): δ=7.62 (brs, 4H; NH), 7.48 (d, *J*=8.4 Hz, 4H; Ar-H), 7.19 (d, *J*=8.4 Hz, 4H; Ar-H), 7.01 (s, 2H; Ar-H), 5.79 (m, 4H; pyrrole-H), 5.76 (m, 4H; pyrrole-H), 5.36 (s, 2H; *meso*-H), 4.03 (t, *J*=6.6 Hz, 4H; O$CH_2C_{15}H_{31}$), 2.21 (s, 12H; CH_3), 1.84 (quin, *J*=6.6 Hz, 4H; $OCH_2CH_2C_{14}H_{29}$), 1.46 (m, 4H; $OC_2H_4CH_2C_{13}H_{27}$), 1.37–1.26 (m, 48H; $OC_3H_6C_{12}H_{24}CH_3$), 0.88 ppm (t, *J*=6.6 Hz, 6H; $OC_{15}H_{30}CH_3$); MALDI-TOF-MS: *m*/*z* (%): calcd for $C_{76}H_{102}N_4O_2$: 1102.80 $[M]^+$; found: 1102.8 (100), 1103.7 (58).

4,5-Bis(4-dipyrrilylphenylethynyl)-1,2-dihexadecyloxybenzene (2a): Dipyrromethane **s6a** (666 mg, 0.63 mmol) was dissolved in THF (40 mL) and stirred in an ice bath. DDQ (317 mg, 1.4 mmol) in THF (30 mL) was added slowly dropwise over the course of 35 min. DDQ was removed by alumina column and the solution was evaporated. The residue was purified by silica gel column chromatography (Wakogel C-300; 3% MeOH/CH_2Cl_2) and GPC column with THF to afford **2a** as a yellow solid (430 mg, 0.41 mmol, 65%). R_f=0.38 (3% MeOH/CH_2Cl_2); ^{1}H NMR (600 MHz, $CDCl_3$, 20°C; see also the Supporting Information, Figure S10): δ=7.65–7.64 (m, 8H; Ar-H and pyrrole-H), 7.49 (d, *J*=8.4 Hz, 4H; Ar-H), 7.08 (s, 2H; Ar-H), 6.60 (d, *J*=3.6 Hz, 4H; pyrrole-H), 6.38 (d, *J*=4.2 Hz, 4H; pyrrole-H), 4.06 (t, *J*=6.6 Hz, 4H; O$CH_2C_{15}H_{31}$), 1.88 (m, 4H; $OCH_2CH_2C_{14}H_{29}$), 1.38–1.26 (m, 52H; $OC_2H_4C_{13}H_{26}CH_3$), 0.88 ppm (t, *J*=6.6 Hz, 6H; $OC_{15}H_{30}CH_3$); UV/Vis (CH_2Cl_2): λ_{max} (ε)= 432.5 nm (3.7×10^4 M^{-1}cm^{-1}); MALDI-TOF-MS: *m*/*z* (%): calcd for $C_{72}H_{90}N_4O_2$: 1042.71 $[M]^+$; found 1042.7 (100), 1043.7 (80), 1044.7 (35).

4,5-Bis(4-(5,5′-dimethyldipyrrilyl)phenylethynyl)-1,2-dihexadecyloxybenzene (2b): Dipyrromethane **s6b** (162 mg, 0.15 mmol) was dissolved in THF (10 mL) and stirred in an ice bath. DDQ (74 mg, 0.33 mmol) in THF (10 mL) was added slowly dropwise over the course of 35 min. DDQ was removed by alumina column and the solution was evaporated. The residue was purified by silica gel column chromatography (Wakogel C-300; EtOAc/*n*-hexane=3/7) to afford **2b** as a yellow solid (22.7 mg, 0.07 mmol, 49%). R_f=0.42 (5% MeOH/CH_2Cl_2); ^{1}H NMR (600 MHz, $CDCl_3$, 20°C; see also the Supporting Information, Figure S11): δ=7.62 (d, *J*=8.4 Hz, 4H; Ar-H), 7.45 (d, *J*=8.4 Hz, 4H; Ar-H), 7.06 (s, 2H; Ar-H), 6.45 (d, *J*=4.2 Hz, 4H; pyrrole-H), 6.14 (d, *J*=4.2 Hz, 4H; pyrrole-H), 4.07 (t, *J*=6.6 Hz, 4H; O$CH_2C_{15}H_{31}$), 2.48 (s, 12H; CH_3), 1.88 (quin, *J*=6.6 Hz, 4H; $OCH_2CH_2C_{14}H_{29}$), 1.50 (m, 4H; $OC_2H_4CH_2C_{13}H_{27}$), 1.37–1.26 (m, 48H; $OC_3H_6C_{12}H_{24}CH_3$), 0.88 ppm (t, *J*=6.6 Hz, 6H; $OC_{15}H_{30}CH_3$); UV/Vis (CH_2Cl_2): λ_{max} (ε)=445.5 nm (4.9×10^4 M^{-1}cm^{-1}); MALDI-TOF-MS: *m*/*z* (%): calcd for $C_{76}H_{98}N_4O_2$: 1098.76 $[M]^+$; found: 1098.8 (100), 1099.7 (80), 1100.7 (20).

[*n*+*n*]-Type Zn^{II} complex of 2a, $2a_n$·Zn^{II}_n: $Zn(OAc)_2$·$2H_2O$ (8.34 mg, 0.038 mmol) was added to dipyrrin **2a** (40 mg, 0.038 mmol) in THF (12 mL) and the solution was stirred for 8 h. The reaction mixture was diluted with $CHCl_3$ (40 mL), washed with saturated aqueous Na_2CO_3 (30 mL) and brine (30 mL), and then dried over $MgSO_4$ and evaporated to afford $\mathbf{2a}_n$·Zn^{II}_n (*n*=2 and 3 as a mixture) as an orange solid. See the details in the ^{1}H NMR spectra (600 MHz, $CDCl_3$, 20°C; the Supporting Information, Figure S12) and FT-ICR-MS (the Supporting Information, Figure S12); elemental analysis calcd (%) for $(C_{72}H_{88}N_4O_2Zn)_n$: C 78.13, H 8.01, N 5.06; found: C 78.26, H 8.13, N 5.04.

[2+2]-Type Zn^{II} complex of 2b, $2b_2$·Zn^{II}_2: $Zn(OAc)_2$·$2H_2O$ (2.2 mg, 0.010 mmol) was added to dipyrrin **2b** (10 mg, 0.010 mmol) in THF (3.3 mL) and the solution was stirred for 6 h. The reaction mixture was diluted with $CHCl_3$ (20 mL), washed with saturated aqueous Na_2CO_3 (20 mL) and brine (20 mL), and then dried over $MgSO_4$ and evaporated. The residue was purified by GPC column with toluene and by GPC-HPLC, and recrystallized from $CHCl_3$/MeOH to afford $\mathbf{2b}_2$·Zn^{II}_2 as an orange solid (4.1 mg, 1.8 μmmol, 36%). Higher oligomers were also obtained (see also the Supporting Information, Figure S13a). R_f=0.45 (CH_2Cl_2/*n*-hexane=1:1); m.p. 235°C (decomp); ^{1}H NMR (600 MHz, $CDCl_3$, 20°C; see also the Supporting Information, Figure S14): δ=7.53 (d, *J*=7.8 Hz, 8H; Ar-H), 7.35 (d, *J*=7.8 Hz, 8H; Ar-H), 7.07 (s, 4H; Ar-H), 6.47 (d, *J*=4.2 Hz, 8H; pyrrole-H), 5.92 (d, *J*=4.2 Hz, 8H; pyrrole-H), 4.08 (t, *J*=6.6 Hz, 8H; O$CH_2C_{15}H_{31}$), 1.94 (s, 24H; CH_3), 1.87 (quin, *J*=7.2 Hz, 8H; $OCH_2CH_2C_{14}H_{29}$), 1.50 (m, 8H; $OC_2H_4CH_2C_{13}H_{27}$), 1.39–1.25 (m, 96H; $OC_3H_6C_{12}H_{24}CH_3$), 0.88 ppm (t, *J*=6.6 Hz, 12H; $OC_{15}H_{30}CH_3$); UV/Vis (CH_2Cl_2): λ_{max} (ε)=513 nm (16×10^4 M^{-1}cm^{-1}); FT-ICR-MS (MALDI): *m*/*z* (%): calcd for $C_{152}H_{192}N_8O_4Zn_2$: 2321.36 $[M]^+$; found 2321.3 (32), 2322.3 (54), 2323.3 (68), 2324.3 (75), 2325.3 (100), 2326.3 (93), 2327.3 (80), 2328.3 (60), 2329.3 (45), 2330.3 (28), 2331.3 (14), 2332.3 (9); elemental analysis calcd (%) for $C_{152}H_{192}N_8O_4Zn_2$: C 78.49, H 8.32, N 4.82; found: C 78.25, H 8.44, N 4.62.

[3+3]-Type Zn^{II} complex of 2b, $2b_3$·Zn^{II}_3: $Zn(OAc)_2$·$2H_2O$ (2.2 mg, 0.010 mmol) was added to dipyrrin **2b** (10 mg, 0.010 mmol) in THF (3.3 mL) and the solution was stirred for 6 h. After this time, the reaction mixture was diluted with $CHCl_3$ (20 mL), washed with saturated aqueous Na_2CO_3 (20 mL) and brine (20 mL), and then dried over $MgSO_4$ and evaporated. The residue was purified by GPC column with toluene and by GPC-HPLC, and recrystallized from $CHCl_3$/MeOH to afford $\mathbf{2b}_3$·Zn^{II}_3 as an orange solid (3.1 mg, 0.9 μmmol, 27%). Higher oligomers were also obtained (see the Supporting Information, Figure S13a). R_f=0.50 (CH_2Cl_2/*n*-hexane=1:1); m.p. 130°C (c.p. 230°C); ^{1}H NMR (600 MHz, $CDCl_3$, 20°C; see also the Supporting Information, Figure S16): δ=7.66 (d, *J*=8.4 Hz, 12H; Ar-H), 7.51 (d, *J*=8.4 Hz, 12H; Ar-H), 7.09 (s, 6H; Ar-H), 6.57 (d, *J*=3.6 Hz, 12H; pyrrole-H), 6.18 (d, *J*=4.2 Hz, 12H; pyrrole-H), 4.08 (t, *J*=6.6 Hz, 12H; O$CH_2C_{15}H_{31}$), 2.08 (s, 36H; CH_3), 1.89 (quin, *J*=7.2 Hz, 12H; $OCH_2CH_2C_{14}H_{29}$), 1.51 (m, 12H;

$OC_2H_4CH_2C_{13}H_{27}$), 1.38–1.26 (m, 144H; $OC_3H_6C_{12}H_{24}CH_3$), 0.89 ppm (t, $J=6.6$ Hz, 18H; $OC_{15}H_{30}CH_3$); UV/Vis (CH_2Cl_2): λ_{max} (ε) = 491.5 nm (2.0×10^4 M^{-1}cm^{-1}); FT-ICR-MS (MALDI): *m/z* (%): calcd for $C_{228}H_{288}N_{12}O_6Zn_3$: 3482.05 $[M]^+$; found 3482.7 (35), 3483.7 (52), 3484.7 (74), 3485.7 (88), 3486.7 (95), 3487.8 (100), 3488.7 (96), 3489.7 (90), 3490.7 (83), 3491.7 (75), 3492.7 (52), 3493.7 (35), 3494.7 (23), 3495.7 (18), 3496.1 (15); elemental analysis calcd (%) for $C_{228}H_{288}N_{12}O_6Zn_3\cdot3H_2O$: C 77.29, H 8.36, N 4.74; found: C 76.22, H 8.19, N 4.49.

[*n*+*n*]-Type Ni^{II} complex of 2a, 2a$_n$·Ni$^{II}_n$: $Ni(OAc)_2\cdot4H_2O$ (11.91 mg, 0.047 mmol) was added to dipyrrin **2a** (50 mg, 0.047 mmol) in THF (16 mL) and the solution was stirred for 5 h. After this time, the reaction mixture was diluted with $CHCl_3$ (30 mL), washed with saturated aqueous Na_2CO_3 (30 mL) and brine (30 mL), and then dried over $MgSO_4$ and evaporated to afforded **2a**$_n$·Ni$^{II}_n$ as a mixture including mainly **2a**$_n$·Ni$^{II}_n$ as a red solid. See the details in the ^{1}H NMR spectrum (600 MHz, $CDCl_3$, 20 °C: the Supporting Information, Figure S16) and FT-ICR-MS (the Supporting Information, Figure S13); elemental analysis calcd (%) for $(C_{72}H_{88}N_4NiO_2)_n$: C 78.60, H 8.06, N 5.09; found: C 77.29, H 7.96, N 5.05.

[2+2]-Type Ni^{II} complex of 2b, 2b$_2$·Ni$^{II}_2$: $Ni(OAc)_2\cdot4H_2O$ (11.19 mg, 0.045 mmol) was added to dipyrrin **2b** (49 mg, 0.045 mmol) in THF (15 mL) and the solution was stirred for 12 h. After this time, the reaction mixture was diluted with $CHCl_3$ (30 mL), washed with saturated aqueous Na_2CO_3 (20 mL) and brine (20 mL), and then dried over $MgSO_4$ and evaporated. The residue was purified by GPC-HPLC and recrystallized from $CHCl_3$/MeOH to afford **2b**$_2$·Ni$^{II}_2$ as a red solid (7.7 mg, 3.3 μmmol, 15%). Higher oligomers were also obtained (see also the Supporting Information, Figure S13b). R_f = 0.36 (CH_2Cl_2/*n*-hexane = 1:1); m.p. 124 °C (c.p. 214 °C); ^{1}H NMR (600 MHz, $CDCl_3$, 20 °C; see also the Supporting Information, Figure S17): δ = 64.78 (s, 8H; pyrrole-H), 42.08 (s, 24H; CH_3), 5.76 (s, 4H; Ar-H), 3.56 (s, 8H; $OCH_2C_{15}H_{31}$), 3.23 (s, 8H; Ar-H), 1.25–0.77 (m, 124H; $OCH_2C_{15}H_{31}$), 0.14 (s, 8H; Ar-H), −10.52 ppm (s, 8H; pyrrole-H); UV/Vis (CH_2Cl_2): λ_{max} (ε) = 515.0 nm (0.6×10^4 M^{-1}cm^{-1}); FT-ICR-MS (MALDI): *m/z* (%): calcd for $C_{152}H_{192}N_8O_4Ni_2$: 2309.38 $[M]^+$; found 2309.4 (6), 2310.4 (33), 2311.4 (55), 2312.4 (80), 2313.4 (88), 2314.4 (100), 2315.4 (95), 2316.4 (77), 2317.4 (59), 2318.4 (39), 2319.4 (23), 2320.4 (12), 2321.4 (9); elemental analysis calcd (%) for $C_{152}H_{192}N_8Ni_2O_4\cdot4H_2O$: C 76.56, H 8.45, N 4.70; found: C 77.75, H 8.56, N 4.40.

[3+3]-Type Ni^{II} complex of 2b, 2b$_3$·Ni$^{II}_3$: $Ni(OAc)_2\cdot4H_2O$ (11.19 mg, 0.045 mmol) was added to dipyrrin **2b** (49 mg, 0.045 mmol) in THF (15 mL) and the solution was stirred. After 12 h, the reaction mixture was diluted with $CHCl_3$ (30 mL), washed with saturated aqueous Na_2CO_3 (20 mL) and brine (20 mL), and then dried over $MgSO_4$ and evaporated. The residue was purified by GPC-HPLC and recrystallized from $CHCl_3$/MeOH to afford **2b**$_3$·Ni$^{II}_3$ as a red solid (12.5 mg, 3.6 μmmol, 24%). Higher oligomers were also obtained (see also the Supporting Information, Figure S13b). R_f = 0.46 (CH_2Cl_2/*n*-hexane = 1:1); m.p. 120 °C (c.p. 223 °C); ^{1}H NMR (600 MHz, $CDCl_3$, 20 °C; see also the Supporting Information, Figure S18): δ = 63.71 (s, 12H; pyrrole-H), 41.15 (s, 36H; CH_3), 5.63 (s, 12H; Ar-H), 3.33 (s, 12H; $OCH_2C_{15}H_{31}$) 3.16 (s, 12H; Ar-H), 1.25–0.81 (m, 186H; $OCH_2C_{15}H_{31}$), −0.07 (s, 12H; Ar-H), −10.28 ppm (s, 12H; pyrrole-H); UV/Vis (CH_2Cl_2): λ_{max} (ε) = 514.0 nm (1.4×10^4 M^{-1}cm^{-1}); FT-ICR-MS (MALDI): *m/z* (%): calcd for $C_{228}H_{288}N_{12}O_6Ni_3$: 3464.07 $[M]^+$; found 3464.1 (20), 3465.1 (43), 3466.1 (65), 3467.1 (88), 3468.1 (100), 3469.1 (98), 3470.1 (86), 3471.1 (71), 3472.1 (53), 3473.1 (36), 3474.1 (24), 3475.1 (16), 3476.1 (12), 3477.1 (9); elemental analysis calcd (%) for $C_{228}H_{288}N_{12}Ni_3O_6\cdot6H_2O$: C 76.56, H 8.45, N 4.70; found: C 76.57, H 8.55, N 4.38.

Zn^{II} complex of 1,9-dimethyl-5-phenyldipyrrin (3), 3$_2$·Zn^{II}: $Zn(OAc)_2\cdot2H_2O$ (88.39 mg, 0.41 mmol) was added to a THF solution (20 mL) of 1,9-dimethyl-5-phenyldipyrrin **3**[11] (200 mg, 0.81 mmol) and the solution was stirred for 1 h. After this time, the reaction mixture was diluted with CH_2Cl_2 (40 mL), washed with saturated aqueous Na_2CO_3 (30 mL) and brine (30 mL), and then dried over $MgSO_4$ and evaporated. The residue was recrystallized from CH_2Cl_2/MeOH to afford **3**$_2$·Zn^{II} as an orange solid (193.3 mg, 0.34 mmol, 86%). R_f = 0.63 (CH_2Cl_2/*n*-hexane = 1:2); ^{1}H NMR (600 MHz, $CDCl_3$, 20 °C): δ = 7.49–7.39 (m, 10H; Ar-H), 6.55 (d, $J=4.2$ Hz, 4H; pyrrole-H), 6.18 (d, $J=4.2$ Hz, 4H; pyrrole-H), 2.11 ppm (s, 12H; pyrrole-CH_3); UV/Vis (CH_2Cl_2): λ_{max} (ε) = 490.5 nm (13×10^4 M^{-1}cm^{-1}); MALDI-TOF-MS: *m/z* (%): calcd for $C_{34}H_{30}N_2Zn$: 558.18 $[M]^+$; found 558.2 (100), 559.2 (40), 560.2 (70), 561.2 (40), 562.2 (45), 563.2 (20).

Ni^{II} complex of 3, 3$_2$·Ni^{II}: $Ni(OAc)_2\cdot4H_2O$ (16.7 mg, 0.07 mmol) was added to dipyrrin **3**[11] (33.9 mg, 0.14 mmol) in THF (10 mL) and the solution was stirred for 1 h. After this time, the reaction mixture was diluted with CH_2Cl_2 (30 mL), washed with saturated aqueous Na_2CO_3 (10 mL) and brine (10 mL), and then dried over $MgSO_4$ and evaporated. The residue was purified by silica gel column chromatography (Wakogel C-300; CH_2Cl_2) to afford **3**$_2$·Ni^{II} as a red solid (31.8 mg, 0.056 mmol, 83%). R_f = 0.55 (CH_2Cl_2); ^{1}H NMR (600 MHz, $CDCl_3$, 20 °C): δ = 63.00 (brs, 4H; pyrrole-H), 40.53 (s, 12H; pyrrole-CH_3), 5.02 (brs, 2H; Ar-H), 4.02 (brs, 4H; Ar-H), −0.17 (brs, 4H; Ar-H), −10.07 ppm (br, 4H; pyrrole-H); UV/Vis (CH_2Cl_2): λ_{max} (ε) = 513.0 nm (6.3×10^4 M^{-1}cm^{-1}); MALDI-TOF-MS: *m/z* (%): calcd for $C_{34}H_{30}N_2Ni$: 552.18 $[M]^+$; found: 552.2 (100), 553.2 (50), 554.2 (30).

Method for single-crystal X-ray analysis: Crystallographic data for metal complexes of dypyrins are summarized in Table 2. A single crystal of **1a**$_2$·Zn$^{II}_2$ was obtained by vapor diffusion of hexane into a dichloromethane solution. The data crystal was a red prism of approximate dimensions 0.60 mm × 0.30 mm × 0.10 mm. Data were collected at 123 K on a Rigaku RAXIS-RAPID diffractometer with graphite-monochromated $Mo_{K\alpha}$ radiation (λ = 0.71075 Å), and structure was solved by direct methods. A single crystal of **1b**$_3$·Zn$^{II}_3$ was obtained by vapor diffusion of *n*-hexane into a chlorobenzene solution. The data crystal was an orange prism of approximate dimensions 0.50 mm × 0.10 mm × 0.10 mm. Data were collected at 93 K on a Rigaku RAXIS-RAPID diffractometer with graphite monochromated $Cu_{K\alpha}$ radiation (λ = 1.54187 Å), and structure was solved by direct method. In each compound, the non-hydrogen atoms were refined anisotropically. The calculations were performed using the Crystal Structure crystallographic software package of Molecular Structure Corporation.[12] CIF files (CCDC-895942 (**1a**$_2$·Zn$^{II}_2$) and 895943 (**1b**$_3$·Zn$^{II}_3$)) contain the supplementary crystallographic data for this paper. These data can be obtained free of charge from The Cambridge Crystallographic Data Centre via www.ccdc.cam.ac.uk/data_request/cif.

Table 2. Crystallographic details for compounds **1a**$_2$·Zn$^{II}_2$ and **1b**$_3$·Zn$^{II}_3$.

	1a$_2$·Zn$^{II}_2$	**1b**$_3$·Zn$^{II}_3$
formula	$C_{80}H_{48}N_8Zn_2\cdot3CH_2Cl_2$	$C_{132}H_{96}N_{12}Zn_3$
F_w	1506.78	2046.38
crystal size [mm]	0.60 × 0.30 × 0.10	0.50 × 0.10 × 0.10
crystal system	triclinic	triclinic
space group	$P\bar{1}$ (no. 2)	$P\bar{1}$ (no. 2)
a [Å]	13.337(4)	18.573(5)
b [Å]	15.329(6)	19.128(4)
c [Å]	17.617(7)	19.537(5)
α [°]	95.008(14)	79.59(10)
β [°]	99.879(12)	71.92(11)
γ [°]	97.430(13)	72.08(11)
V [Å^3]	3506(2)	6250(3)
ρ_{calcd} [g cm^{-3}]	1.427	1.087
Z	2	2
T [K]	123(2)	93(2)
μ [mm^{-1}]	0.966 ($Mo_{K\alpha}$)	1.052 ($Cu_{K\alpha}$)
reflns	32918	59286
unique reflns	15497	17165
variables	892	1391
λ [Å]	0.71075 ($Mo_{K\alpha}$)	1.54187 ($Cu_{K\alpha}$)
R_1 [$I>2\sigma(I)$]	0.0741	0.1130
wR_2 [$I>2\sigma(I)$]	0.1846	0.2995
GOF	1.000	1.450

DFT and semiempirical calculations: Ab initio and semi-empirical calculations of metal-bridged macrocycles were carried out by using Gaussian 03 program[5a] and a DELL OPTIPLEX 960 computer. The structures were optimized, and the total electronic energies were calculated at the B3LYP level by using a 6–31G(d,p) basis set for **1a**$_2$·Zn$^{II}_2$, **1b**$_2$·Zn$^{II}_2$, and **1b**$_3$·Zn$^{II}_3$ and at the PM6 level for **1a**$_2$·Ni$^{II}_2$, **1b**$_2$·Ni$^{II}_2$, and **1b**$_3$·Ni$^{II}_3$. In addition, single-point calculations in solution state at B3LYP/6–31G(d,p) level were carried out by using the Gaussian 09 program[5b] and the RIKEN Integrated Cluster of Clusters (RICC) facility.

Differential scanning calorimetry (DSC): The phase transition points were observed by using a differential scanning calorimetry (Perkin–Elmer Diamond DSC).

Polarizing optical microscopy (POM): POM measurements were carried out with a Nikon OPTIPHOT-POL polarizing optical microscope equipped with a Mettler FP82 HT hot stage.

Synchrotron X-ray diffraction analysis (XRD): High-resolution XRD analyses were carried out using a synchrotron radiation X-ray beam with a wavelength of 1.00 Å on BL40B2 at SPring-8 (Hyogo, Japan).

Flash-photolysis time-resolved microwave conductivity (FP-TRMC): Polycrystalline solid films of **1a**$_2$·Zn$^{II}_2$ and **1b**$_3$·Zn$^{II}_3$ were casted onto quartz substrate at 6~11 μm thick (measured by a Dektak 150 surface profiler from Veeco Instruments Inc.), and excited at 355 nm from a Spectra Physics INDI-HG nanosecond Nd:YAG laser to inject photo-carriers. The power density of the excitation light sources was set at 5.4 mJ cm^{-2} (9.6×10^{15} photons cm^{-2}). Probing microwave at 9.108 GHz, 3 mW was used for the TRMC measurement. The TRMC signals were monitored upon excitation and averaged over 128 shots. Transmittance of excitation light pulses at 355 nm for the film was measured by PE25 power meter of Ophir Optoronics Ltd. All of the above experiments were carried out at 296 K with the microwave cavity filled with Ar or O_2 atmospheres. The microwave power reflection from the cavity (ΔP_r) was picked with a diode and recorded on a digital oscilloscope (Tektronix, TDS 3032B). The relative changes in the microwave power reflection ($\Delta P_r/P_r$, P_r: steady-reflected microwave power) was directly converted into the transient photoconductivity ($\Delta\sigma$), leading into a product of photo-carrier injection yield (ϕ) and the sum of the mobilities of charge carriers ($\Sigma\mu$) as shown in Equation (1):

$$A\frac{\Delta P_r}{P_r} = \Delta\sigma = e\phi N\sum\mu \qquad (1)$$

in which the terms A, e, and N represent the sensitivity factor, elementary charge of the electron, and the number of absorbed photons per unit volume, respectively. The details of the set of apparatus are described elsewhere.[8b, 13]

Determination of quantum efficiency of photo-carrier generation: Photocurrent accumulation was carried out for polycrystalline solid films of **1a**$_2$·Zn$^{II}_2$ and **1b**$_3$·Zn$^{II}_3$ cast onto an Au interdigitated electrode with 5 μm gap. Excitation was carried out at 355 nm with the photon density of 2.3×10^{15} photons cm^{-2} from a Spectra Physics, Quanta-Ray GCR-130, and under a variety of applied bias voltage, photo-current transients were accumulated directly by a Keithley 6514 electrometer, and by monitoring with Tektronix 3052B digital oscilloscope via an evolution with 30 kΩ terminate resistance. The details of the set of apparatus are described elsewhere.[9c,14]

Acknowledgements

This work was supported by PRESTO/JST (2007–2011), Grant-in-Aid for Scientific Research on Innovation Areas ("Coordination Programming" Area 2107, No. 22108533 and 24108740) from the MEXT, and Ritsumeikan R-GIRO project (2008–2013). We thank Prof. Atsuhiro Osuka, Dr. Naoki Aratani, and Mr. Tomohiro Higashino, Kyoto University, for single-crystal X-ray analysis, Dr. Noboru Ohta, JASRI/SPring-8, for synchrotron XRD analysis (BL40B2: 2011B1535), Prof. Tomonori Hanasaki, Ritsumeikan University, for preliminary DSC and POM measurements, Prof. Hikaru Takaya and Dr. Katsuhiro Isozaki, Kyoto University, for FT-ICR-MS measurements carried out in the JURC at ICR, the RIKEN Integrated Cluster of Clusters (RICC) for the computer resources, and Prof. Hitoshi Tamiaki, Ritsumeikan University, for various measurements. Y.B. thanks the JSPS for a Research Fellowship for Young Scientists.

[1] a) *Transition Metals in Supramolecular Chemistry*, (Ed.: J.-P. Sauvage), Wiley, Chichester, **1999**; b) *Metal-Containing and Metallosupramolecular Polymers and Materials*, (Eds.: U. S. Schubert, G. R. Newkome, I. Manners), ACS Symposium Series, 928, Washington DC, **2006**.

[2] a) A. Semenov, J. P. Spatz, M. Möller, J. M. Lehn, B. Sell, D. Schubert, C. H. Weidl, U. S. Schubert, *Angew. Chem.* **1999**, *111*, 2701–2705; *Angew. Chem. Int. Ed.* **1999**, *38*, 2547–2550; b) M. Ruben, J. Rojo, F. J. Romero-Salguero, L. H. Uppadine, J. M. Lehn, *Angew. Chem.* **2004**, *116*, 3728–3747; *Angew. Chem. Int. Ed.* **2004**, *43*, 3644–3662; c) R. Chakrabarty, P. S. Mukherjee, P. J. Stang, *Chem. Rev.* **2011**, *111*, 6810–6918.

[3] a) H. Falk, *The Chemistry of Linear Oligopyrroles and Bile Pigments*, Springer, Vienna, **1989**; b) T. E. Wood, A. Thompson, *Chem. Rev.* **2007**, *107*, 1831–1861; c) S. A. Baudron, *CrystEngComm* **2010**, *12*, 2288–2295.

[4] a) H. Maeda, M. Hasegawa, T. Hashimoto, T. Kakimoto, S. Nishio, T. Nakanishi, *J. Am. Chem. Soc.* **2006**, *128*, 10024–10025; b) H. Maeda, T. Hashimoto, *Chem. Eur. J.* **2007**, *13*, 7900–7907; c) T. Hashimoto, T. Nishimura, J. M. Lim, D. Kim, H. Maeda, *Chem. Eur. J.* **2010**, *16*, 11653–11661; d) metal-coordination helices of alkene-strapped dipyrrins were also reported: H. Maeda, T. Nishimura, R. Akuta, K. Takaishi, M. Uchiyama, A. Muranaka, *Chem. Sci.* **2013**, *4*, 1204–1211; e) metal-coordination polymers of a *meso–meso* directly linked dipyrrin were prepared: H. Maeda, H. Kobayashi, R. Akuta, *J. Porphyrins Phthalocyanines* **2013**, *17*, 86–91.

[5] a) Gaussian 03, Revision C.01, M. J. Frisch, G. W. Trucks, H. B. Schlegel, G. E. Scuseria, M. A. Robb, J. R. Cheeseman, J. A. Montgomery, Jr., T. Vreven, K. N. Kudin, J. C. Burant, J. M. Millam, S. S. Iyengar, J. Tomasi, V. Barone, B. Mennucci, M. Cossi, G. Scalmani, N. Rega, G. A. Petersson, H. Nakatsuji, M. Hada, M. Ehara, K. Toyota, R. Fukuda, J. Hasegawa, M. Ishida, T. Nakajima, Y. Honda, O. Kitao, H. Nakai, M. Klene, X. Li, J. E. Knox, H. P. Hratchian, J. B. Cross, C. Adamo, J. Jaramillo, R. Gomperts, R. E. Stratmann, O. Yazyev, A. J. Austin, R. Cammi, C. Pomelli, J. W. Ochterski, P. Y. Ayala, K. Morokuma, G. A. Voth, P. Salvador, J. J. Dannenberg, V. G. Zakrzewski, S. Dapprich, A. D. Daniels, M. C. Strain, O. Farkas, D. K. Malick, A. D. Rabuck, K. Raghavachari, J. B. Foresman, J. V. Ortiz, Q. Cui, A. G. Baboul, S. Clifford, J. Cioslowski, B. B. Stefanov, G. Liu, A. Liashenko, P. Piskorz, I. Komaromi, R. L. Martin, D. J. Fox, T. Keith, M. A. Al-Laham, C. Y. Peng, A. Nanayakkara, M. Challacombe, P. M. W. Gill, B. Johnson, W. Chen, M. W. Wong, C. Gonzalez, J. A. Pople, Gaussian, Inc., Wallingford CT, **2004**; b) Gaussian 09, Revision B.01, M. J. Frisch, G. W. Trucks, H. B. Schlegel, G. E. Scuseria, M. A. Robb, J. R. Cheeseman, G. Scalmani, V. Barone, B. Mennucci, G. A. Petersson, H. Nakatsuji, M. Caricato, X. Li, H. P. Hratchian, A. F. Izmaylov, J. Bloino, G. Zheng, J. L. Sonnenberg, M. Hada, M. Ehara, K. Toyota, R. Fukuda, J. Hasegawa, M. Ishida, T. Nakajima, Y. Honda, O. Kitao, H. Nakai, T. Vreven, J. A. Montgomery, Jr., J. E. Peralta, F. Ogliaro, M. Bearpark, J. J. Heyd, E. Brothers, K. N. Kudin, V. N. Staroverov, R. Kobayashi, J. Normand, K. Raghavachari, A. Rendell, J. C. Burant, S. S. Iyengar, J. Tomasi, M. Cossi, N. Rega, N. J. Millam, M. Klene, J. E. Knox, J. B. Cross, V. Bakken, C. Adamo, J. Jaramillo, R. Gomperts, R. E. Stratmann, O. Yazyev, A. J. Austin, R. Cammi, C. Pomelli, J. W. Ochterski, R. L. Martin, K. Morokuma, V. G. Zakrzewski, G. A. Voth, P. Salvador, J. J. Dannenberg, S. Dapprich, A. D. Daniels, Ö. Farkas, J. B. Foresman, J. V. Ortiz, J. Cioslowski, D. J. Fox, Gaussian, Inc., Wallingford CT, **2009**.

[6] Q. Miao, J.-Y. Shin, B. O. Patrick, D. Dolphin, *Chem. Commun.* **2009**, 2541–2543.

[7] Organized structures of $\mathbf{2b}_n{\cdot}Zn^{II}_n$ ($n=2$, 3) precipitated from $CHCl_3$/MeOH were not observed by differential scanning calorimetry (DSC), polarized optical microscopy (POM), and synchrotron X-ray diffractions (XRD) (BL40B2 at SPring-8). This is because dipyrin moieties of Zn^{II} complexes were not suitable for the formation of fairly ordered stacking structures due to their orthogonal tetrahedral coordination geometries.

[8] a) S. Seki, S. Tagawa, *Polym. J.* **2007**, *39*, 277–293; b) A. Saeki, Y. Koizumi, T. Aida, S. Seki, *Acc. Chem. Res.* **2012**, *45*, 1193–1202.

[9] a) S. Seki, Y. Yoshida, S. Tagawa, K. Asai, K. Ishigure, K. Furukawa, M. Fujiki, N. Matsumoto, *Philos. Mag. B* **1999**, *79*, 1631–1645; b) B. M. Schmidt, S. Seki, B. Topolinski, K. Ohkubo, S. Fukuzumi, H. Sakurai, D. Lentz, *Angew. Chem.* **2012**, *124*, 11548–11551; *Angew. Chem. Int. Ed.* **2012**, *51*, 11385–11388; c) Y. Yasutani, A. Saeki, T. Fukumatsu, Y. Koizumi, S. Seki, *Chem. Lett.* **2013**, *42*, 19–21.

[10] K. Tahara, S. Furukawa, H. Uji-I, T. Uchino, T. Ichikawa, J. Zhang, W. Mamdouh, M. Sonoda, F. C. De Schryver, S. De Feyter, Y. Tobe, *J. Am. Chem. Soc.* **2006**, *128*, 16613–16625.

[11] W. Qin, M. Baruah, M. V. Den Auweraer, F. C. De Schryver, N. Boens, *J. Phys. Chem. A* **2005**, *109*, 7371–7384.

[12] CrystalStructure (Ver. 3.8), Single Crystal Structure Analysis Software, Rigaku/MSC and Rigaku Corporation, **2006**.

[13] A. Acharya, S. Seki, A. Saeki, Y. Koizumi, S. Tagawa, *Chem. Phys. Lett.* **2005**, *404*, 356–360.

[14] T. Amaya, S. Seki, T. Moriuchi, K. Nakamoto, T. Nakata, H. Sakane, A. Saeki, S. Tagawa, T. Hirao, *J. Am. Chem. Soc.* **2009**, *131*, 408–409.

Received: May 27, 2013
Published online: July 12, 2013

